Supporting Information

Non-oxidative methane conversion by Fe single site catalysts: quantifying temperature limitations imposed by gas-phase pyrolysis

Jongyoon Bae[1], Javad Hashemi[1], Dongmin Yun[2], Do Kyoung Kim[2], Dae Hyun Choo[2], C. Franklin Goldsmith[1,*], and Andrew A. Peterson[1,*]

[1]*Chemical Engineering Group, School of Engineering, Brown University, Providence, RI 02912, USA*
[2]*Institute of Environmental Science and Technology, SK innovation, 325 Expo-ro, Yuseong-gu, Daejeon, Republic of Korea, 34124*

S-1 XRD measurement on synthesized Fe-SSC

The Fe-SSC was sythesized as described in the original work by Guo *et al.* [1]. X-ray diffractograms (XRD) were recorded on a X'Pert PRO instrument (PANalytical) using CuKα radiation (λ = 1.54 Å), operated at 40 kV and 30 mA with a scan rate of 0.01°/sec over a 2θ range of 10–80°. The XRD spectra of synthesized Fe-SSC is shown in Figure S1.

In order to determine the crystal phase of the catalyst at reaction temperatures, the XRD measurements were made at a range of temperatures from 30°C to 1000°C. The result is shown in Figure S2. The dominant crystal phase was β-cristobalite for the temperatures above 300°C.

S-2 Free energy diagram with two silica crystal phases

Energetics of the two Fe single-site catalysts with different silica crystal phases are presented in Figure S3. Overall, the differences in binding energy were less than 0.3 eV and the largest discrepancy was observed in state (v): the surface structure with two hydrogen adsorbates where each hydrogen adsorbed on each surface carbon site.

S-3 Barrier calculation by CFI method

Barrier calculations were conducted using CFI method [2]. In each plot, top pane shows potential energy and bottom pane shows constraint force with the gray band indicating convergence criteria of 0.05 eV/Å. Transition states of the two methane activation steps (Figure S4 and Figure S6) and associative H_2 step (S7) were found. CFI method predicted two different pathways for the

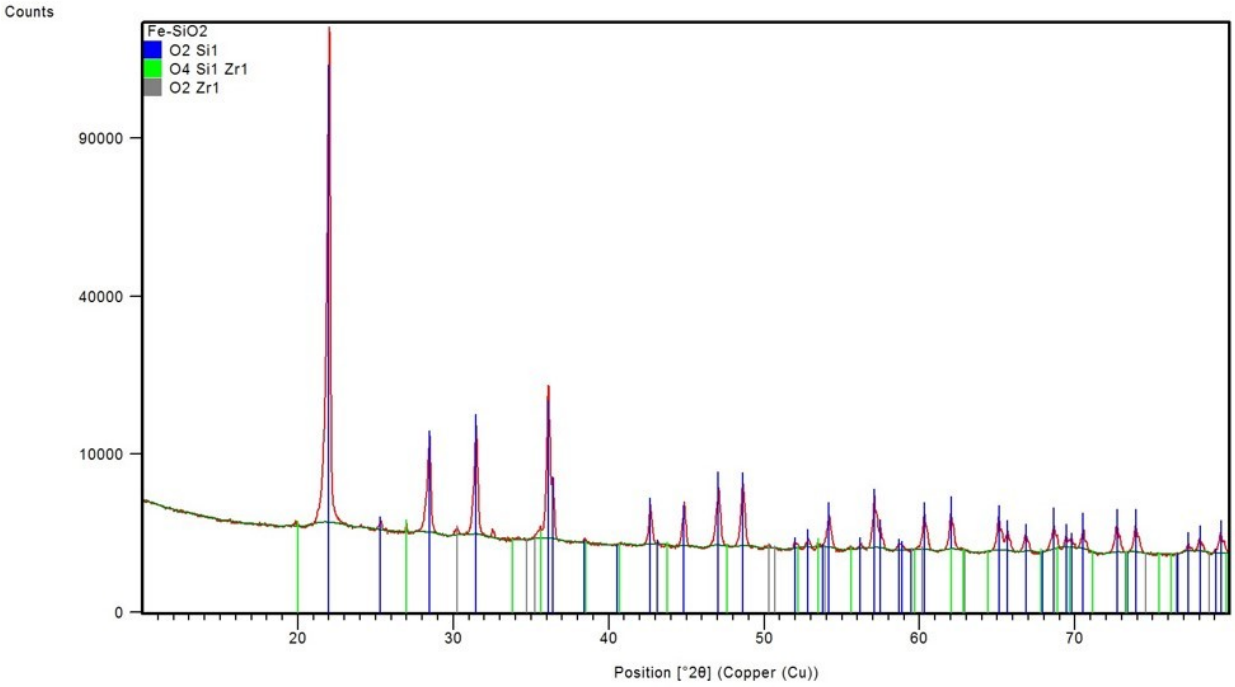

Figure S1: XRD spectra of Fe-SSC. Colored marks indicate β-cristobalite(blue), $ZrSiO_4$(green), and ZrO_2(gray).

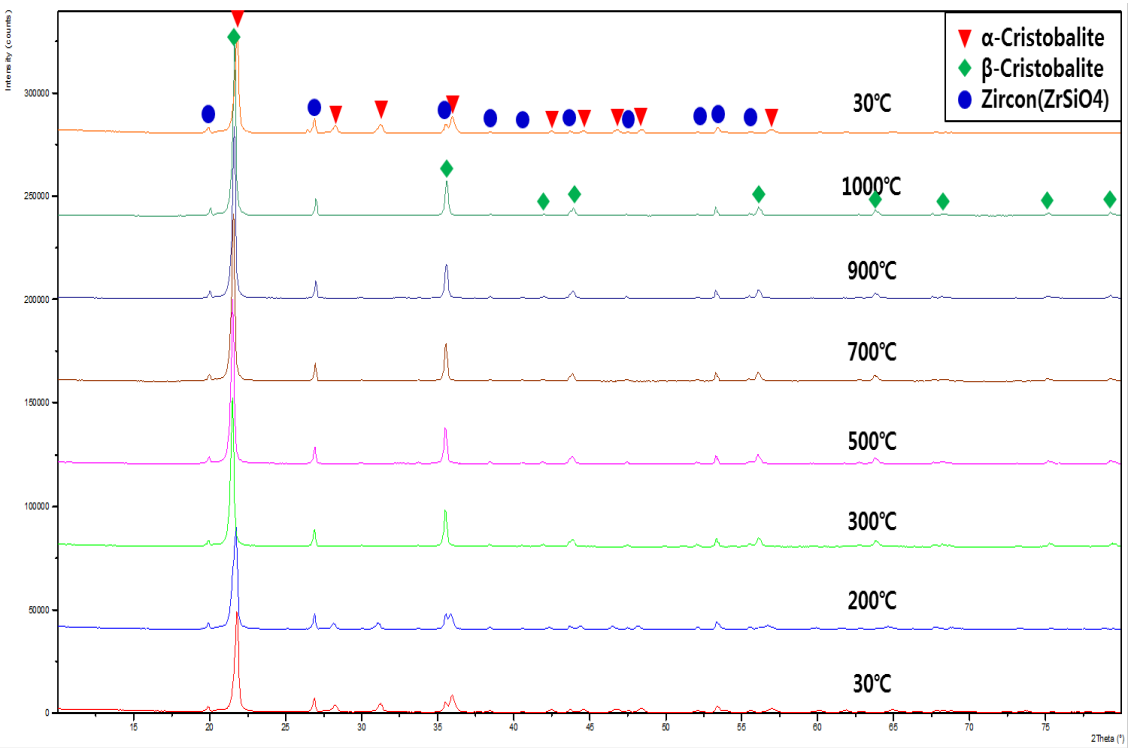

Figure S2: XRD spectra of Fe-SSC taken at different temperatures from 30°C to 1000°C. The top spectra is a spectra of reference materials taken at 30°C.

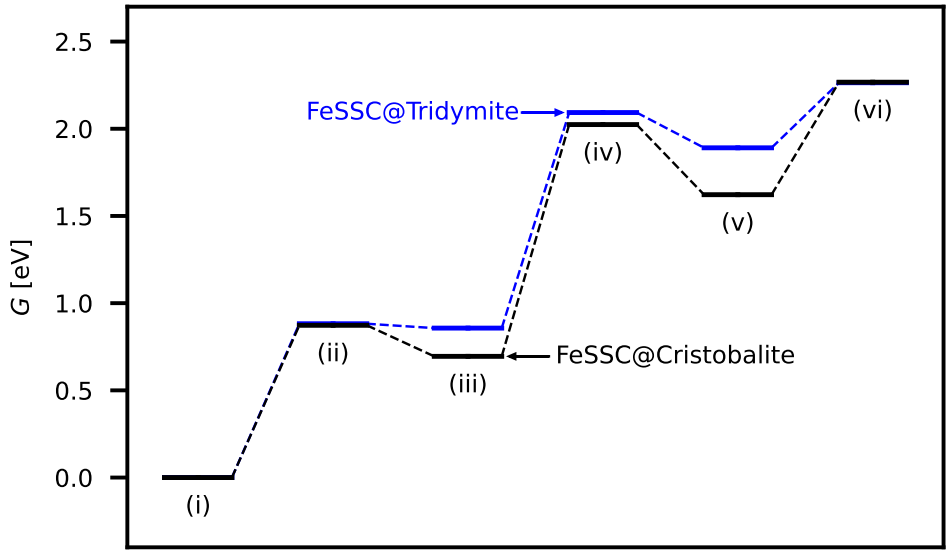

Figure S3: Free energy diagram of surface mechanism on Fe-SSC with β-cristobalite(001) and with β-tridymite(001) at 950°C and 1 atm.

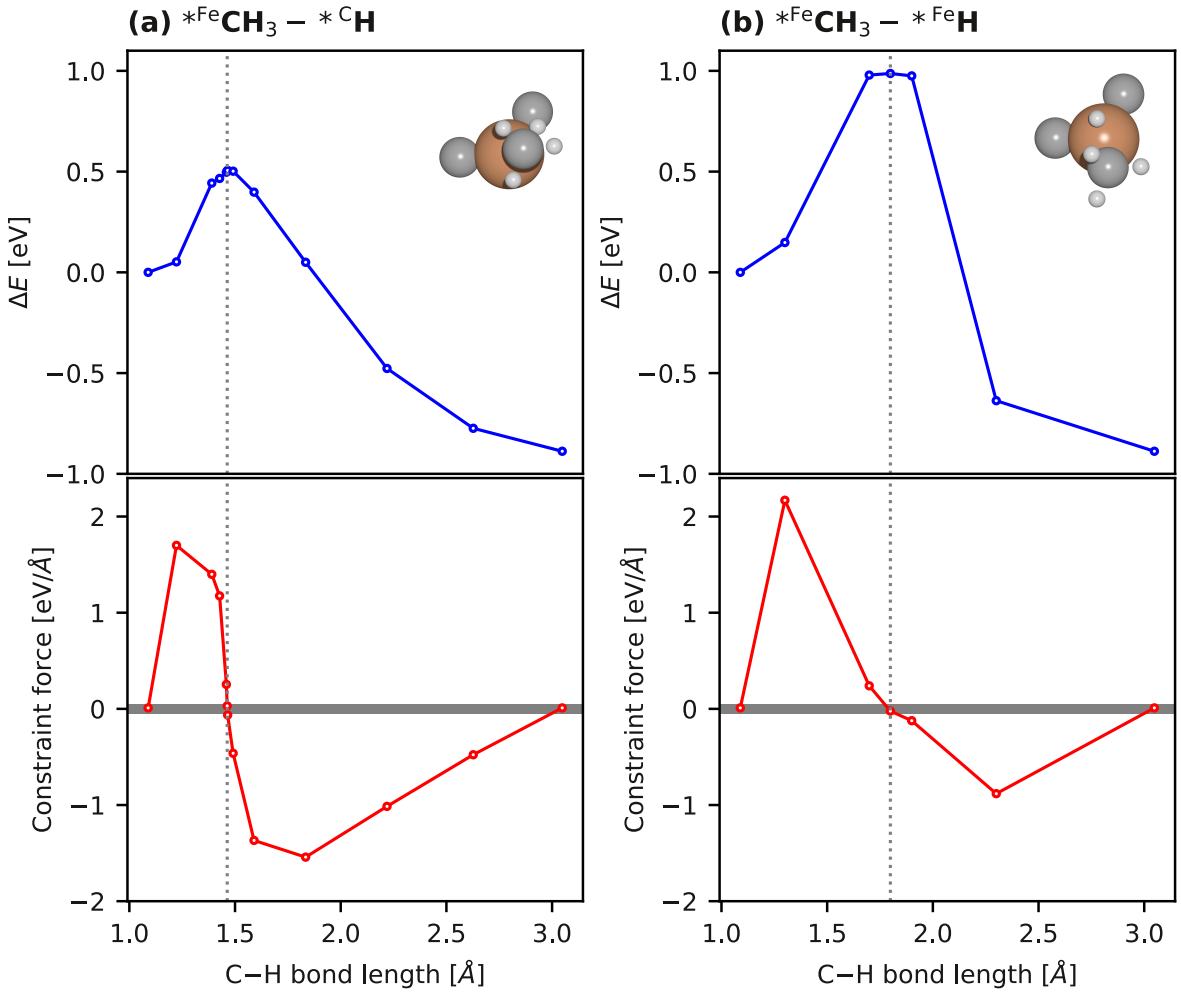

Figure S4: Barrier for the first reaction step in surface mechanism: (a). pathway of C−H dissociation involving both Fe and C sites and (b). pathway of C−H dissociation only on Fe site. Inset images are the catalyst active center and adsorbates at the transition states. Elements in the inset images are Fe (brown), C (gray), and H (white).

methane activation steps and both of the different pathways are shown. Methyl desorption steps were predicted to be barrierless processes (Figure S5), noted by monotonic increase in potential energy as the methyl desorbes further away from the Fe site.

S-4 Effective ΔG of barrierless desorption

The Equations of k^{TST} and k^{des} are compared and solved for the effective free energy barrier of desorption in Equation (S1).

$$\Delta G^{\ddagger,\mathrm{effective}} = -k_{\mathrm{B}}T \ln\left[\frac{h}{k_{\mathrm{B}}T}\frac{S_c^{\circ}}{\Gamma}\left(\frac{k_{\mathrm{B}}T}{2\pi m}\right)^{1/2} e^{\frac{\Delta G_{\mathrm{des}}}{RT}}\left(\frac{P^{\circ}}{RT}\right)^{-1}\right] \tag{S1}$$

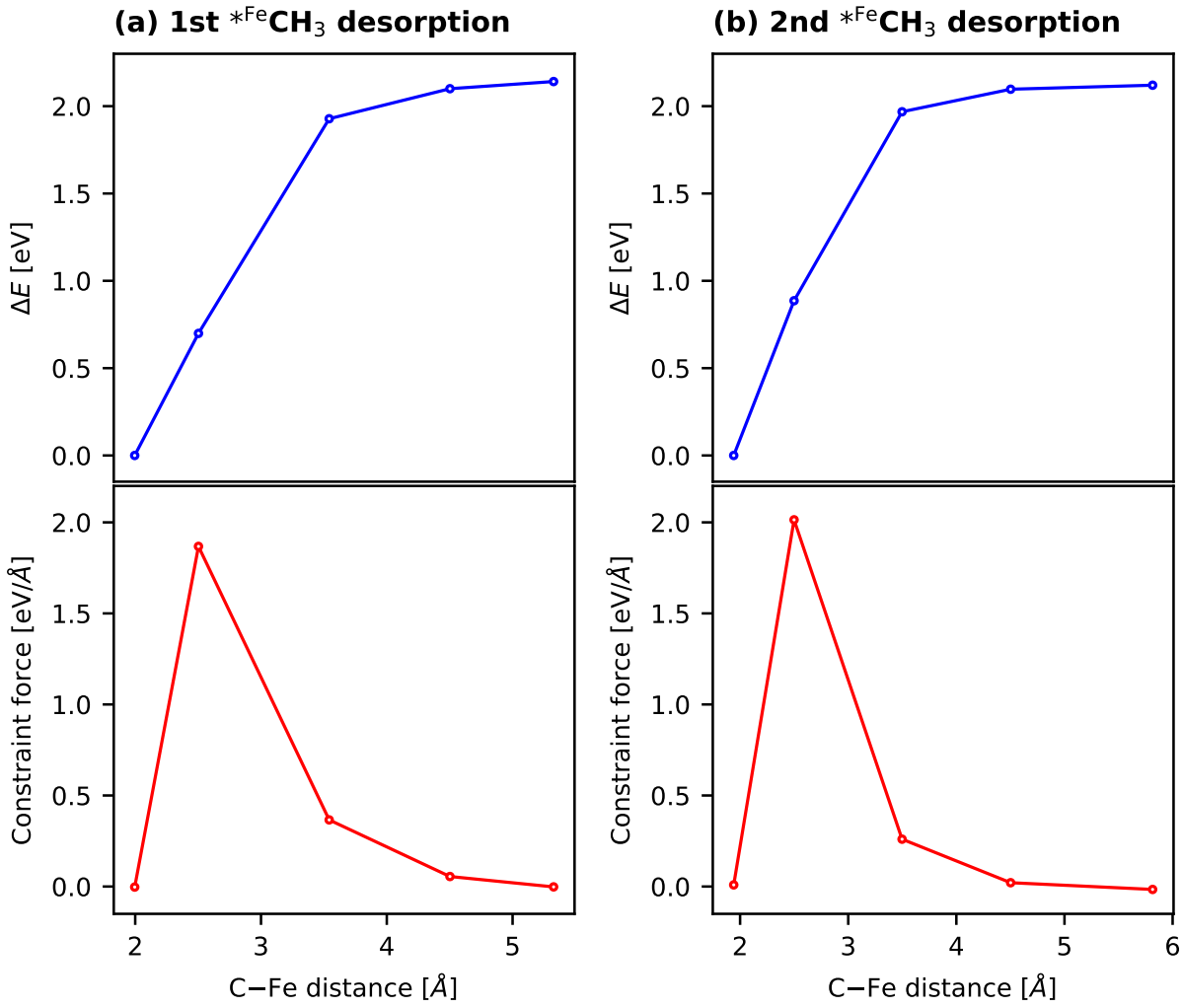

Figure S5: Potential energy and constraint force diagrams for the second and fourth reaction steps in surface mechanism: (a). first methyl radical desorption and (b). second methyl radical desorption.

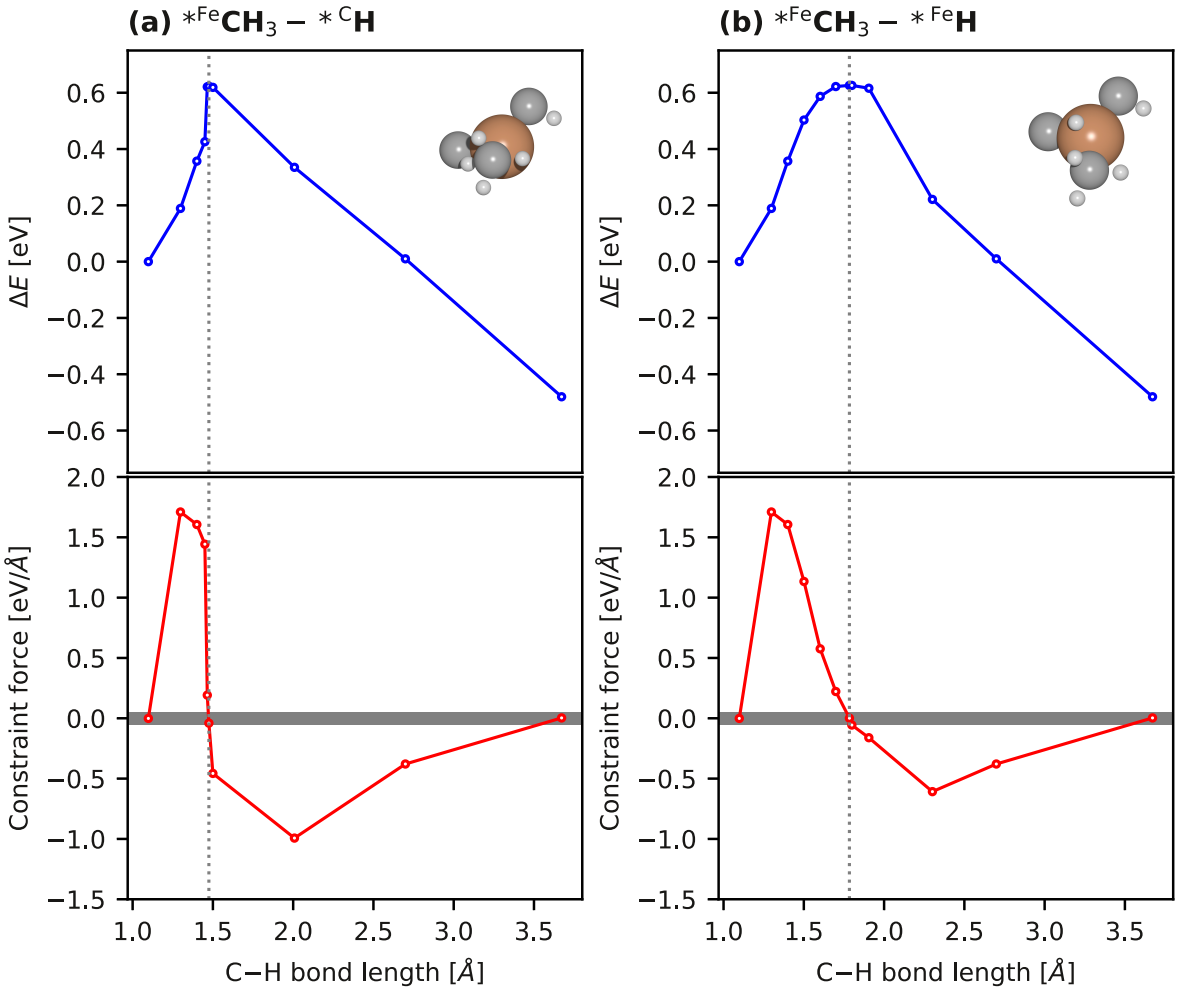

Figure S6: Barrier for the third reaction step in surface mechanism: (a). pathway of C−H dissociation involving both Fe and C sites and (b). pathway of C−H dissociation only on Fe site. Inset images are the catalyst active center and adsorbates at the transition states. Elements in the inset images are Fe (brown), C (gray), and H (white).

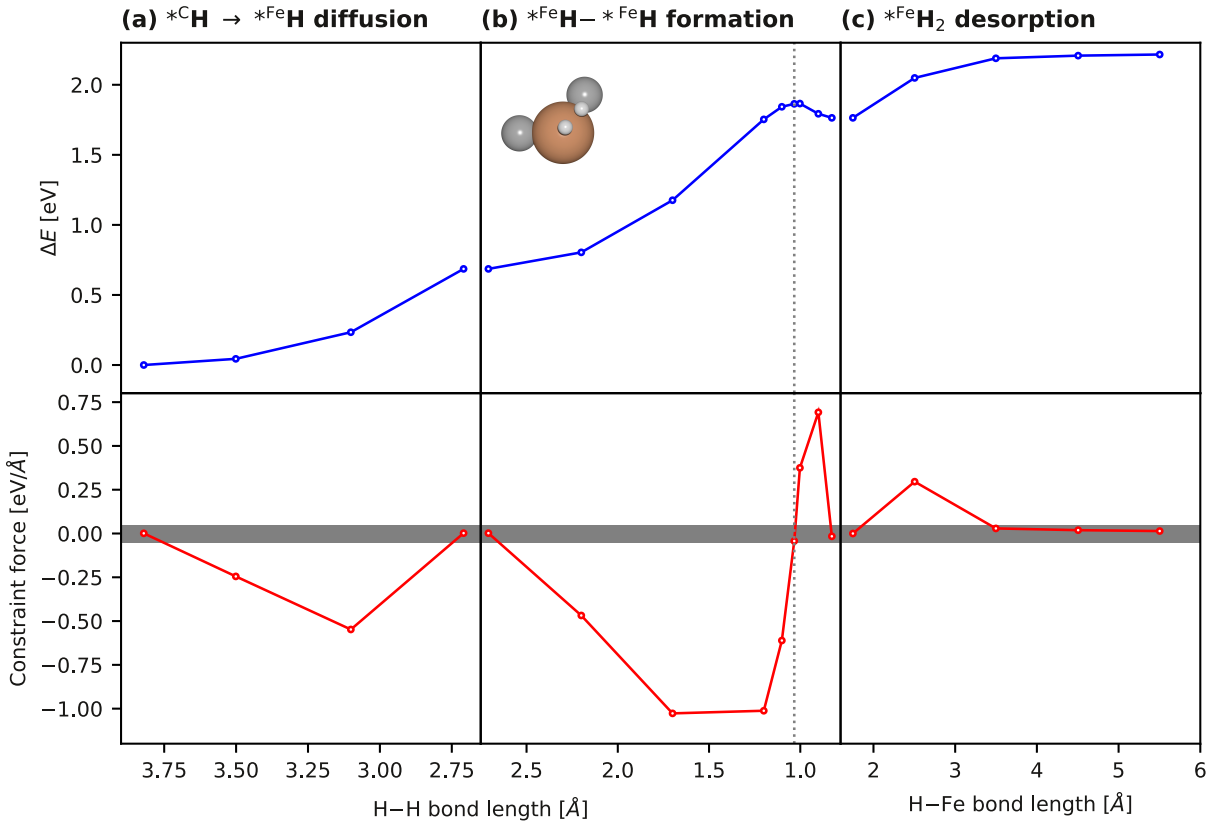

Figure S7: Barrier for the fifth elementary step in surface mechanism: associative H_2 desorption. (a). H adsorbate diffusion from C site to Fe site, (b). H−H formation, and (c). H_2 desorption. Inset image is the catalyst active center and adsorbates at the transition state. Elements in the inset image are Fe (brown), C (gray), and H (white).

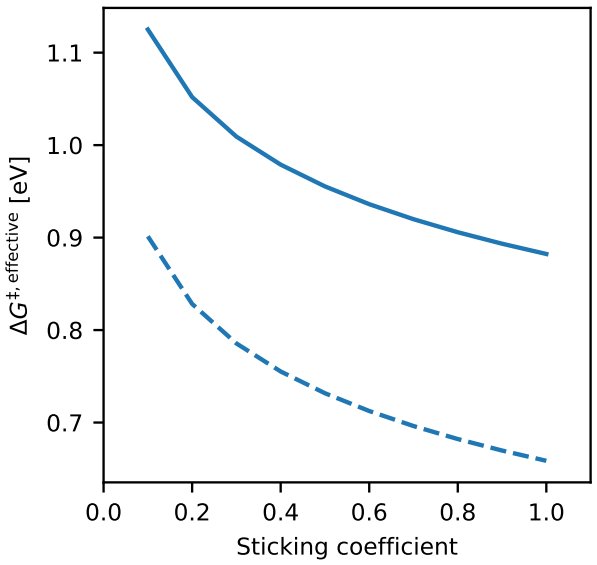

Figure S8: Effective free energy barrier heights of first (solid) and second (dashed) methyl desorption steps as a function of sticking coefficients at 950°C.

S-5 Desorption barrier height sensitivity on sticking coefficient

As described in the Equation S1, calculated free energy barrier height of methyl desorption is directly impacted by the sticking coefficient. We assumed methyl sticking coefficient of 0.9 for our calculations. To evaluated how sensitive the desorption barrier height to the sticking coefficient, the barrier energy was calculated using different sticking coefficients ranging from 0.1 to 1.0 at 950°C. The result is shown in S8.

S-6 PFR simulation as a series of different number of CSTRs

To efficiently model a PFR reactor as a series of CSTRs, PFR represented with three different numbers of CSTRs were simulated and compared. PFR simulation results with 1000 CSTRs, 500 CSTRs, and 100 CSTRs are shown in Figure S9. The close overlap between 1000 CSTRs profile and 500 CSTRs profile demonstrate PFR representation with 500 CSTRs is appropriate.

S-7 Adsorbates and gaseous species in alternative pathways

The species at each state in the proposed methyl pathway as well as two alternative pathways (Figure 6) of methylene pathway and H radical pathway are listed below.

1. Methyl pathway

   state (i): $*^{\mathrm{Fe}} + 2\,*^{\mathrm{C}} + 2\,\mathrm{CH_4}$

   state (ii): $*^{\mathrm{Fe}}\mathrm{CH_3} + *^{\mathrm{C}}\mathrm{H} + *^{\mathrm{C}} + \mathrm{CH_4}$

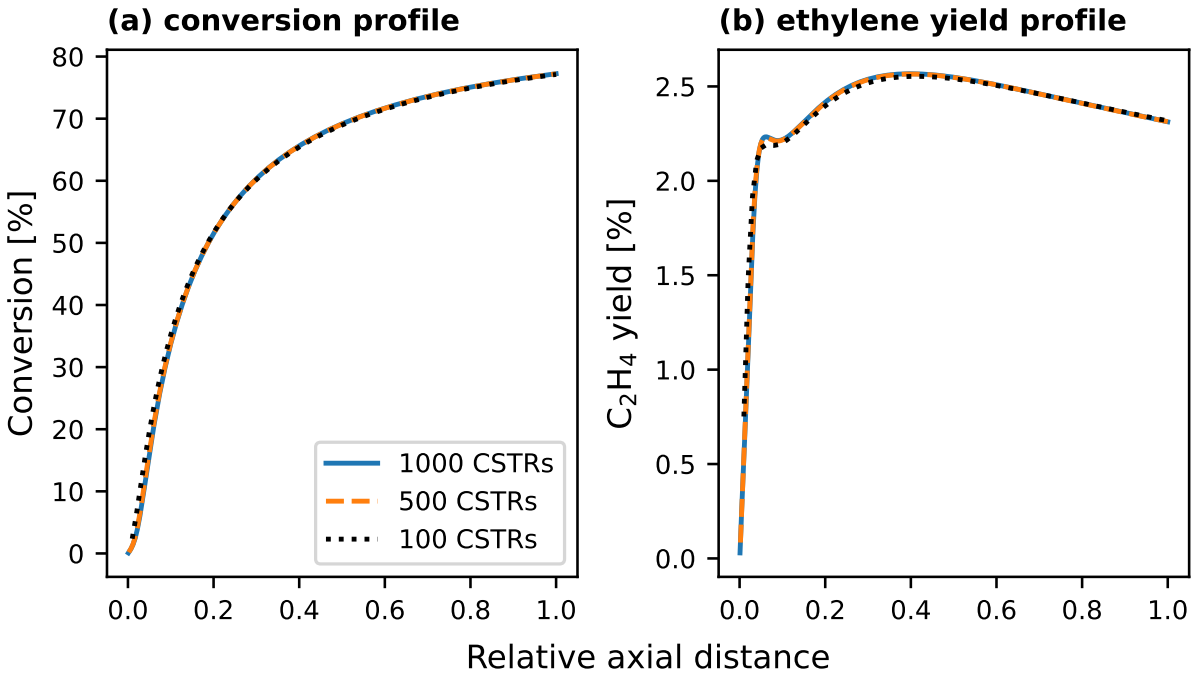

Figure S9: PFR simulations results of non-catalytic NOCM with different number of CSTRs to model single PFR: (a). conversion profile and (b). ethylene yield profile at 1200°C, 1 atm, and GHSV of 1316 hr^{-1} with equimolar methane/nitrogen inlet.

state (iii): $*^{Fe} + *^{C}H + *^{C} + CH_3 + CH_4$
state (iv): $*^{Fe}CH_3 + *^{C}H*^{C}H + CH_3$
state (v): $*^{Fe} + *^{C}H*^{C}H + 2\,CH_3$
state (vi): $*^{Fe} + 2*^{C} + 2\,CH_3 + H_2$

2. Methylene pathway

state (i): $*^{Fe} + 2*^{C} + 2\,CH_4$
state (ii): $*^{Fe}CH_3 + *^{C}H + *^{C} + CH_4$
state (iii)-b: $*^{Fe}CH_2 + *^{C}H*^{C}H + CH_4$
state (iv)-b: $*^{Fe} + *^{C}H*^{C}H + CH_2 + CH_4$
state (v)-b: $*^{Fe} + 2*^{C} + CH_2 + H_2 + CH_4$
state (vi)-b: $*^{Fe}CH_3 + *^{C}H + CH_2 + H_2$
state (vii)-b: $*^{Fe}CH_2 + *^{C}H*^{C}H + CH_2 + H_2$
state (viii)-b: $*^{Fe} + *^{C}H*^{C}H + 2\,CH_2 + H_2$
state (ix)-b: $*^{Fe} + 2*^{C} + 2\,CH_2 + 2\,H_2$

3. H radical pathway

state (i): $*^{Fe} + 2*^{C} + 2\,CH_4$

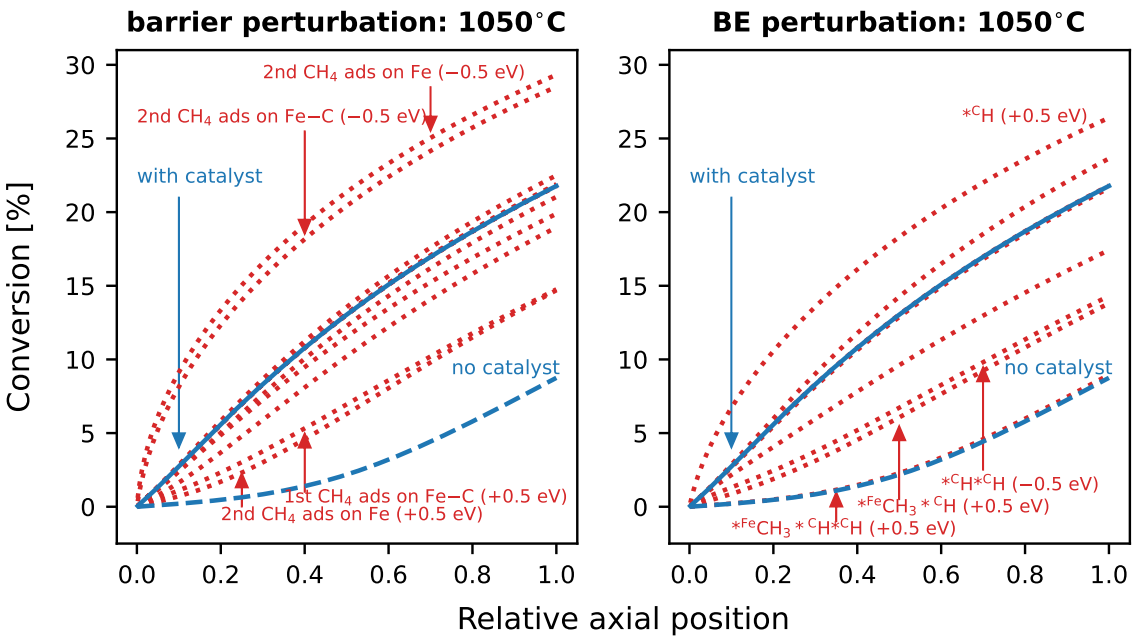

Figure S10: Sensitivity analysis at 1050°C, 1 atm, and GHSV: 1316 hr^{-1}. Unperturbed conversion profile with (solid blue line) and without Fe-SSC (dashed blue line) are shown as reference. Dotted red lines show the conversion profiles with (a). Fe-SSC for barrier energy perturbations and (b). binding energy (BE) perturbations. Either one barrier energy or one binding energy was perturbed by ±0.5 eV at a time.

state (ii): $*^{Fe}CH_3 + *^{C}H + *^{C} + CH_4$

state (iii): $*^{Fe} + *^{C}H + *^{C} + CH_3 + CH_4$

state (iv)-c: $*^{Fe} + 2*^{C} + CH_3 + H + CH_4$

state (v)-c: $*^{Fe}CH_3 + *^{C}H + *^{C} + CH_3 + H$

state (vi)-c: $*^{Fe} + *^{C}H + *^{C} + 2\,CH_3 + H$

state (vii)-c: $*^{Fe} + 2*^{C} + 2\,CH_3 + 2\,H$

state (viii)-c: $*^{Fe} + 2*^{C} + C_2H_6 + 2\,H$

S-8 Barrier and binding energy sensitivity analysis

Each of total seven reactions (2 × first methane adsorption, 1 × first methyl desorption, 2 × second methane adsorption, 1 × second methyl desorption, 1× H_2 desorption) and four surface species ($*^{Fe}CH_3 + *^{C}H$,$*^{C}H$, $*^{Fe}CH_3 + *^{C}H*^{C}H$, $*^{C}H$) binding energies was perturbed by ±0.5 eV. The perturbed profiles are shown in Figure S10 where only the those with noticeable deviation from unperturbed are labeled.

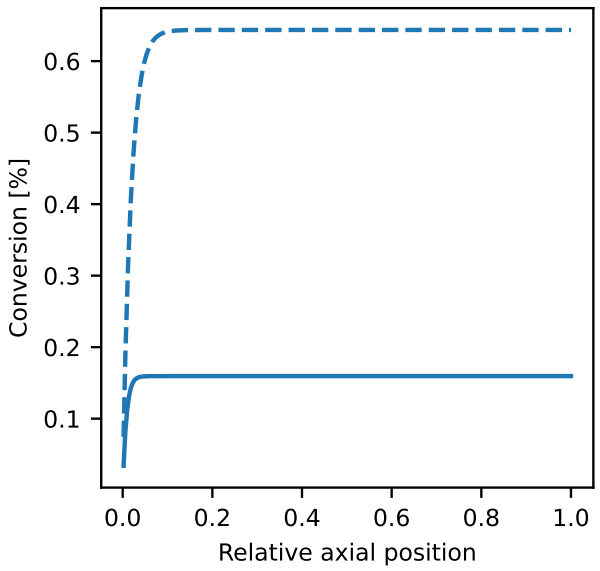

Figure S11: Catalytic model without gas-phase reactions in PFR at 1 atm, GHSV of 1316 hr^{-1}, 1050°C (solid), and 1200°C (dashed) with equimolar methane/nitrogen inlet.

S-9 Detailed mole fractions of PFR simulation exit stream

The PFR simulations with and without catalyst were conducted at three different temperatures of 900°C, 1050°C, and 1200°C. Inlet stream was 50%:50% CH_4:N_2 by volume, and GHSV (gas hourly space velocity) was 1316 hr^{-1} at 1 atm. The detailed compositions of the six simulations are listed in Table S1.

S-10 Catalytic PFR simulation in the absence of gas-phase reactions

To assess how much methane is converted catalytically when no gas-phase reactions are present in the model, only the surface mechanism was used to simulate PFR. Therefore all of the converted methane became methyl and H_2 and no other gas-phase species were present except the inert N_2 in Figure S11.

S-11 Non-catalytic gas-phase simulations

Non-catalytic gas-phase simulation were conducted for the same conditions as those of Figure 10 and the results are shown in Figure S12.

AUTHOR INFORMATION

Corresponding authors. *Email: franklin_goldsmith@brown.edu. Telephone +1 401-863-6468. *Email: andrew_peterson@brown.edu. Telephone +1 401-863-2153.

900°C, no catalyst	CH_4	H_2	C_2H_2	C_2H_4	C_2H_6
(conversion: 0.00%)	50%	50 ppm	0.66 ppm	11 ppm	25 ppm
	C_3H_4	C_4H_2	C_6H_6	C_7H_8	C_8H_6
	0.00 ppm	0.00 ppm	0.01%	0.00 ppm	0.00 ppm
	C_9H_8	$C_{10}H_8$	$C_{12}H_8$		
	0.00 ppm	0.00 ppm	0.00 ppm		
900°C, with catalyst	CH_4	H_2	C_2H_2	C_2H_4	C_2H_6
(conversion: 3.4%)	48%	1.9%	0.09%	0.43%	0.06%
	C_3H_4	C_4H_2	C_6H_6	C_7H_8	C_8H_6
	0.06%	9.7 ppm	85 ppm	7.9 ppm	0.00 ppm
	C_9H_8	$C_{10}H_8$	$C_{12}H_8$		
	0.00 ppm	0.00 ppm	0.00 ppm		
1050°C, no catalyst	CH_4	H_2	C_2H_2	C_2H_4	C_2H_6
(conversion: 8.8%)	44%	5.9%	0.54%	0.30%	0.028%
	C_3H_4	C_4H_2	C_6H_6	C_7H_8	C_8H_6
	0.15%	0.028	0.18%	0.043%	44 ppm
	C_9H_8	$C_{10}H_8$	$C_{12}H_8$		
	10 ppm	3.7 ppm	0. 00 ppm		
1050°C, with catalyst	CH_4	H_2	C_2H_2	C_2H_4	C_2H_6
(conversion: 22%)	36%	14%	1.3%	0.62%	0.02%
	C_3H_4	C_4H_2	C_6H_6	C_7H_8	C_8H_6
	0.16%	0.062%	0.64%	0.069%	0.024%
	C_9H_8	$C_{10}H_8$	$C_{12}H_8$		
	0.014%	98 ppm	16 ppm		
1200°C, no catalyst	CH_4	H_2	C_2H_2	C_2H_4	C_2H_6
(conversion: 77%)	8.8%	46%	2.5%	0.45%	31 ppm
	C_3H_4	C_4H_2	C_6H_6	C_7H_8	C_8H_6
	0.045%	0.051%	1.5%	0.021%	0.045%
	C_9H_8	$C_{10}H_8$	$C_{12}H_8$		
	0.052%	0.21%	0.91%		
1200°C, with catalyst	CH_4	H_2	C_2H_2	C_2H_4	C_2H_6
(conversion: 77%)	8.8%	46%	2.5%	0.45%	31 ppm
	C_3H_4	C_4H_2	C_6H_6	C_7H_8	C_8H_6
	0.044%	0.051%	1.5%	0.021%	0.045%
	C_9H_8	$C_{10}H_8$	$C_{12}H_8$		
	0.052%	0.21%	0.92%		

Table S1: Outlet stream mole fractions of PFR simulation with and without catalyst at 1 atm and GHSV of 1316 hr^{-1}.

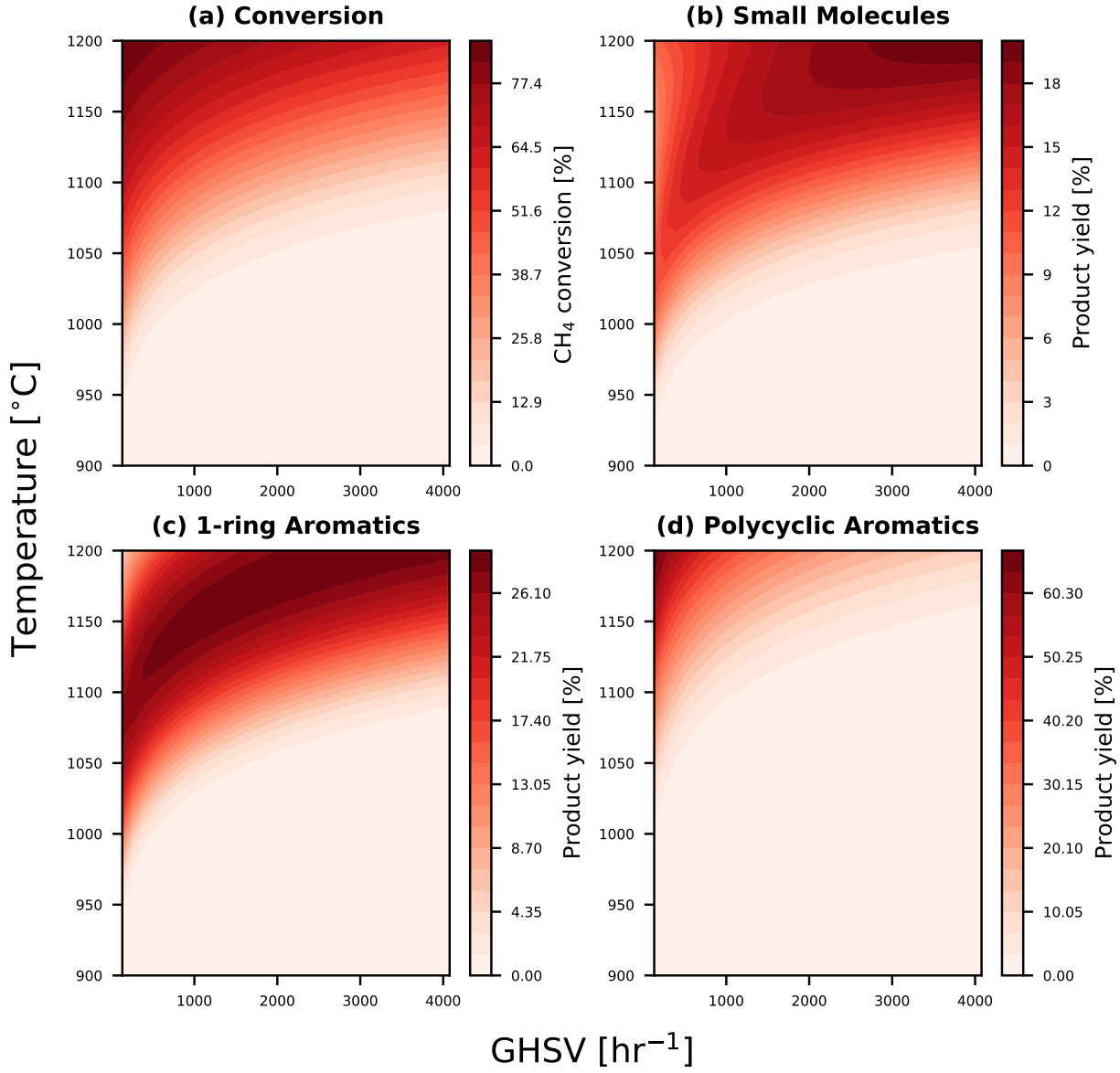

Figure S12: Contour plots of gas-phase only mechanism PFR simulations result showing (a). conversion and (b–d). product yields.

References

[1] Guo, X.; Fang, G.; Li, G.; Ma, H.; Fan, H.; Yu, L.; Ma, C.; Wu, X.; Deng, D.; Wei, M.; Tan, D.; Si, R.; Zhang, S.; Li, J.; Sun, L.; Tang, Z.; Pan, X.; Bao, X. Direct, Nonoxidative Conversion of Methane to Ethylene, Aromatics, and Hydrogen. *Science* **2014**; 344, 616–619.

[2] Bae, J.; Goldsmith, C.F.; Peterson, A.A. in preparation **2022**; .